

Temperature-Dependent Exciton Dynamics in CdTe Quantum Dot Superlattices Fabricated via Layer-by-Layer Assembly

メタデータ	言語: English 出版者: Wiley 公開日: 2023-06-01 キーワード (Ja): キーワード (En): layer-by-layer assembly, minibands, photoluminescence dynamics, quantum dot superlattices, quantum resonance, temperature dependence 作成者: 李, 太起, 大城, 一馬, 渡辺, 太一, 金, 賢得, 金, 大貴 メールアドレス: 所属: Osaka City University, Osaka City University, Osaka City University, Kyoto University, Osaka City University
URL	https://ocu-omu.repo.nii.ac.jp/records/2019595

Temperature-Dependent Exciton Dynamics in CdTe Quantum Dot Superlattices Fabricated via Layer-by-Layer Assembly

TaeGi Lee, Kazuma Ohshiro, Taichi Watanabe, Kim Hyeon-Deuk,
DaeGwi Kim

Citation	Advanced Optical Materials. 10(11); 2102781
Issue Date	2022-06-03
Version of Record	2022-05-25
Type	Journal Article
Textversion	Author
Supporting Information	Supporting Information is available at https://doi.org/10.1002/adom.202102781 .
Rights	This is the peer reviewed version of the following article: Advanced Optical Materials. Volume 10, Issue 11, 2102781, which has been published in final form at https://doi.org/10.1002/adom.202102781 . This article may be used for non-commercial purposes in accordance with Wiley Terms and Conditions for Use of Self-Archived Versions. This article may not be enhanced, enriched or otherwise transformed into a derivative work, without express permission from Wiley or by statutory rights under applicable legislation. Copyright notices must not be removed, obscured or modified. The article must be linked to Wiley's version of record on Wiley Online Library and any embedding, framing or otherwise making available the article or pages thereof by third parties from platforms, services and websites other than Wiley Online Library must be prohibited.
DOI	10.1002/adom.202102781

Self-Archiving by Author(s)
Placed on: Osaka City University

**Temperature-dependent exciton dynamics in CdTe quantum dot superlattices
fabricated via layer-by-layer assembly**

*TaeGi Lee, Kazuma Ohshiro, Taichi Watanabe, Kim Hyeon-Deuk, and DaeGwi Kim**

T.G. Lee, K. Ohshiro, T. Watanabe, Prof. D. Kim

Department of Applied Physics, Osaka City University, Osaka 558-8585, Japan

E-mail: tegi@a-phys.eng.osaka-cu.ac.jp

Kim H.-D.

Department of Chemistry, Kyoto University, Kyoto 606-8502, Japan

Keywords: quantum dot superlattice, layer-by-layer assembly, quantum resonance, miniband, temperature dependence, PL dynamics

The formation of minibands in quantum dot (QD) superlattices (SLs) dramatically increases the mobility of carriers, giving a new way to apply QDs for optoelectronic devices. In previous studies on QDSLs, only a few studies have investigated the temperature dependence of the photoluminescence (PL) properties of QDSLs focusing on the formation of miniband. Here, we propose a new model that simultaneously considers the extended and localized exciton states formed in the QDSLs to clarify the PL mechanism of QDSLs. By systematically investigating the temperature dependence of absorption, PL spectra, and PL decay profiles in CdTe QDSLs, we found that the Stokes shift becomes smaller and the PL decay time of the miniband edge PL becomes longer with an increase in temperature. The elucidated PL mechanism of QDSLs will help clarifying further photoexcited dynamics and their physical mechanism intrinsically appearing in the QDSLs with the miniband.

1. Introduction

Short-range resonant coupling (*i.e.*, the quantum resonance) occurs between adjacent quantum dots (QDs) because of the electronic coupling of the wave functions in a QD superlattice (SL) where QDs are regularly arranged.^[1,2] Delocalized excitonic states (minibands) that extend throughout the QDSL are formed when the quantum resonance occurs in the QDSLs.^[1,3] The change in excitonic states caused by the quantum resonance should cause changes in the optical and charge transport properties of the QDSL.^[3-6] In fact, the formation of minibands dramatically improves the charge transport properties.^[3,5,6] Lee *et al.* reported an electron mobility as high as $16 \text{ cm}^2/\text{Vs}$ in the arrays of CdSe/CdS colloidal QDs.^[5] Thus, it is important to understand the properties and functionalities of QDSLs in which minibands are formed for designing optoelectronic devices using QDSLs such as solar cells,^[7-10] photodetectors,^[11-13] and field effect transistors.^[14,15]

Thus far, the formation of minibands in QDSLs has been discussed in terms of charge transport properties and its temperature dependence.^[5,6,16-18] It is also possible to investigate the formation of minibands based on their optical properties because absorption and photoluminescence (PL) properties change when minibands are formed. Such optical measurements are advantageous for evaluating the intrinsic properties of QDSLs because they do not require any preparation of device structures such as electrode junction.

Several methods have been proposed for arranging QDs synthesized by hot injection method: solvent evaporation, solvent destabilization, and assembly at air-liquid interfaces.^[19-22]

However, it is difficult to make QDs close to each other enough to induce the quantum resonance because ligands used in the hot injection method such as trioctylphosphine oxide^[23] and octadecylamine^[24] are too long. One approach to solve the problem is to exchange the long ligands with short ligands such as ethanedithiol,^[25] ethanediamine,^[16] or metal chalcogenide complexes.^[5] However, QDs need to be closer to each other without ligand exchange to investigate the optical properties of QDSLs because the ligand exchange process degrades the PL properties.^[26]

The use of water-soluble QDs is a promising method to make QDs close.^[27-31] It is possible to make QDs closer without ligand exchange because water-soluble QDs can be originally synthesized using short ligands such as *N*-acetyl-L-cysteine (NAC),^[30] thioglycolic acid,^[27-29] and mercaptopropionic acid.^[27,29] In our previous study, we reported that CdTe QDSLs can be fabricated by the layer-by-layer (LBL) assembly of NAC-capped CdTe QDs and polyelectrolytes, and that the quantum resonance was clearly observed between adjacent CdTe QDs.^[32,33] Further, it was recently demonstrated that the dimensions of the quantum

resonance can be controlled by independently changing the distances between QDs in the stacking (out-of-plane) and in-plane directions.^[33] We also experimentally observed the formation of minibands by studying the excitation energy dependence of the PL spectra and the detection energy dependence of the PL-excitation spectra. In this paper, we reveal excitonic dynamics in CdTe QDSLs wherein the one dimensional (1D), two dimensional (2D), and three dimensional (3D) quantum resonance occurs with the miniband formation by systematically investigating the temperature dependence of absorption, PL spectra, and PL decay profiles.

2. Results and Discussion

Figure 1a shows the temperature dependence of the absorption and PL spectra of the 3D CdTe QDSLs. In the 3D CdTe QDSLs, the quantum resonance occurs not only in the stacking direction but also in the in-plane direction, *i.e.*, the 3D quantum resonance appears.^[33] In both of the absorption and PL spectra, the peaks shifted to the lower energy side with an increase in the temperature. Figure 1b shows the temperature dependence of the absorption and PL peak energies. The temperature dependence of the exciton energy in direct-gap semiconductors follows Varshni's empirical law expressed as follows:^[34]

$$E(T) = E_0 - \frac{\alpha T^2}{T + \beta}, \quad (1)$$

where E_0 , α , and β represents the exciton energy at low temperature, temperature coefficient, and Debye temperature, respectively. The solid curve in Figure 1b was obtained by substituting $\alpha = 5.5 \times 10^{-4}$ eV/K and $\beta = 158$ K^[35] into Equation (1). The agreement between the experimental and calculated results indicates that the temperature dependence of the absorption peak energy in the 3D CdTe QDSLs reflects the temperature dependence of the intrinsic band gap energy of CdTe.

The dashed curve shows the calculated result using Equation (1) for the temperature dependence of the PL peak energy; for α and β , the same values as the absorption case were used. In contrast to the absorption peak energy, the discrepancy was observed in the PL peak energy between the calculated and experimental results, and the discrepancy becomes larger at the lower temperature. The inset shows the temperature dependence of the Stokes shift. The Stokes shift is larger at the lower temperature and it decreases with increasing the temperature. Watanabe *et al.* investigated the temperature dependence of the optical properties of film samples in which CdTe QDs were dispersed.^[36] They reported that the Stokes shift is constant and independent of the temperature for film samples with a dilute dispersion of QDs

wherein the quantum resonance does not occur. Therefore, the current temperature dependence of the Stokes shift is considered as a phenomenon intrinsic to QDSLs. Figure 2a shows the detection energy dependence of the PL decay profiles at 80 K in the 3D CdTe QDSLs. The inset shows the PL spectrum at 80 K; the arrows denote the detection energies. The PL decay profiles depend significantly on the detection energy; the lower the detection energy is, the longer is the PL decay profiles. Similarly, as shown in Figure 2b, the PL decay profile at 300 K becomes longer as the detection energy is lowered, as well as at 80 K. However, compared to the 80 K case, the PL decay profiles detected at the lower energy were shorter while those detected at the higher energy became longer at 300 K. Namely, the PL decay profile becomes less sensitive to the detection energy at the higher temperature. The detection-energy and temperature dependence of the PL decay time illustrated in Figures 2a and 2b is qualitatively different from the dispersed CdTe QD case where the PL decay time is almost independent of the temperature and detection energy.^[36] The PL dynamics in the CdTe QDSL is completely different from the PL dynamics occurring in the CdTe QD film. Thus far, the PL dynamics and detection energy dependence of a PL decay profile in a QD solid have been explained by the energy transfer (ET)-based model.^[24,37] Crooker *et al.* investigated the dependence of the PL decay profiles of close-packed assemblies of CdSe QDs, which are monodispersed or polydispersed;^[37] the results were interpreted based on the ET from the smaller QDs to the larger QDs. Miyazaki *et al.* reported the detection energy dependence of the PL decay profiles and its temperature dependence in CdSe/ZnS QD arrays;^[24] they proposed the exciton hopping model based on the Förster-type ET. Previous studies on the PL dynamics in the close-packed QD assemblies discussed their experimental results based on the ET because QDs cannot be brought sufficiently close to each other due to the presence of long carbon chain ligands such as trioctylphosphine oxide and octadecylamine coordinated on the surface of QDs; the quantum resonance between QDs does not occur in such QD assemblies. In fact, the absorption peak energy in the CdSe/ZnS QD array, in which the surface-to-surface distance between QDs was 2.7 nm, was consistent with that of the solution sample of the CdSe/ZnS QDs, meaning that the low-energy shift owing to the quantum resonance was not observed.^[24] In such close-packed QD assemblies, the long-range dipole-dipole interaction is the essence of the QD interaction, and it is reasonable to discuss their PL mechanism based on the ET-based model. The low-energy shift of the absorption peak caused by the quantum resonance were clearly observed in the NAC-capped CdTe QDSL.^[32,33] Furthermore, we previously verified the formation of minibands stemmed from the quantum resonance in the CdTe QDSLs based on

the experimental result that the PL peak energy does not shift even when the excitation energy is varied, and that the peak energy of the PL excitation (PLE) does not shift even when the detection energy is varied.^[33] Figure S1 shows the detection energy dependence of the PLE spectra of the 3D CdTe QDSL at 80 K, 200 K, and RT. The PLE peak did not shift even when the detection energy is varied not only at RT but also at the low temperatures of 80 K and 200 K. These results demonstrate that the quantum resonance occurs and thus the minibands are formed in the broad temperature region. Therefore, it is necessary to interpret the PL mechanism in the CdTe QDSLs in terms of the miniband formation, which is essentially different from the conventional ET-based model.

Before proposing a new model based on the miniband formation, we fabricated bilayer using CdTe QDs with average QD radii of 2.0 and 1.4 nm and investigated the temperature dependence of the ET dynamics between CdTe QDs to verify that our experimental results cannot be explained by the ET-based mechanism. Figure 3a shows the absorption and PL spectrum of the solution sample of CdTe QDs with radii of 2.0 and 1.4 nm, respectively. Since the two spectra overlap sufficiently, the 1.4 and 2.0 nm QDs are expected to act as energy donors (D-QDs) and energy acceptors (A-QDs) in the bilayer, respectively. Therefore, we measured the temperature dependence of the PL spectra and the PL decay profiles of the bilayer. The monolayers of D-QDs and A-QDs were prepared as reference samples. The temperature dependence of their PL spectra and PL decay profiles were also measured. The PL spectra at 80 K are shown in Figure 3b. In comparison with the monolayers of the D-QDs and A-QDs, the PL quenching of the D-QDs and the PL enhancement of the A-QDs were clearly observed in the bilayer, which can be attributed to the ET from the D-QDs to A-QDs. Figure 3c shows the PL decay profiles at 80 K detected at the PL peak of the D-QDs. The PL decay profile of the D-QDs in the bilayer is clearly shorter than that in the D-QD monolayer, indicating that the ET actually occurs in the bilayer. The experimentally observed PL decay profiles show a non-exponential decay. The non-exponential decay in CdTe QDs can be quantitatively analyzed by the sum of a stretched exponential function and a single exponential function.^[36] The open circles in Figure S2 represent the computed result using the same method as in ref. 36. The intensity ratio of the stretched exponential component is ~ 70 % or more. Therefore, we regarded the stretched exponential component as the intrinsic PL decay time. The details of the analysis of the PL decay profiles are provided in the supporting information (Figure S2). Figure 3d shows the temperature dependence of the ET rate (k_{ET}) estimated from the analysis of the PL decay profiles shown in Figure S2; $k_{ET} = 1/\tau_{bilayer} - 1/\tau_{monolayer}$, where $\tau_{bilayer}$ and $\tau_{monolayer}$ are the average PL decay time of the stretched

exponential component $\langle \tau_1 \rangle$ for the bilayer and monolayer, respectively. Figure 3d clearly demonstrates that the ET rate in the bilayer of CdTe QDs is almost independent of temperature. Therefore, the temperature dependence of the PL decay profiles shown in Figures 2a and 2b cannot be explained by the conventional ET-based model. In other words, a new model is required to explain the current PL dynamics in the CdTe QDSL.

As shown in Figure 4a, the minibands are formed in an ideal QDSL, wherein the QDs of uniform size are regularly arranged. However, in a real QDSL, irregularities are caused by the size distribution and the disorder of the arrangement as shown in Figure 4b. In such case, it is known that weakly localized states, the so-called Anderson localization states, are formed on the low-energy side of the minibands.^[38-40] Thus, we consider the PL process originated not only from the minibands but also from the localized states (Figure 4c). The density of states of the Anderson localization states is tailed exponentially, as shown in^[38-40]

$$D(E) = \frac{1}{\sigma} \exp\left(\frac{E-E_{\max}}{\sigma}\right), \quad (2)$$

where σ denotes the tailing parameter, and E_{\max} represents the energy corresponding to the boundary between the minibands and localized states, which is the so-called mobility edge. On one hand, at low temperature, excitons populated in the relatively deep (low energy) localized states mainly contribute to the PL processes. On the other hand, as the temperature rises, the proportion of the excitons populated in the shallower (high energy) localized states and the minibands increases because of the thermal activation to the higher energy localized states from the low energy localized states (Figure 4d). Therefore, the Stokes shift is expected to become smaller at the higher temperature, which agrees well with the inset of Figure 1b.

We analyzed the PL dynamics of the QDSLs at the low temperature by a Monte Carlo simulation with reference to ref. 41 to quantitatively evaluate these considerations. Tackeuchi *et al.* reported the detection energy dependence of the PL decay profiles in InAs QDs with low QD density, without any inter-QD interaction and in an InAs multicoupled QD structure where the inter-QD interaction occurs.^[41] In the InAs QDs with low QD density, the PL decay time does not depend on the detection energy, whereas, in the multicoupled QDs, the PL decay time depends on the detection energy. The higher the detection energy is, the shorter the PL decay time becomes. The PL dynamics was explained by the following rate equation which includes the carrier tunneling from the small QDs to large QDs.

$$\frac{dn(E_i)}{dt} = -\frac{n(E_i)}{\tau_r} - \int_{E_{\min}}^{E_i} \frac{n(E_i)}{\tau_t} D(E) dE + \int_{E_i}^{E_{\max}} \frac{n(E)}{\tau_t} D(E_i) dE, \quad (3)$$

where $n(E_i)$ represents the exciton population in the i th state with energy E_i . τ_r , τ_t , and $D(E_i)$ represent the recombination lifetime, tunneling time, and density of states at state E_i ,

respectively. The first term on the right-hand side represents the recombination process, the second term represents the relaxation process to states on the lower energy side than E_i , and the third term represents the relaxation from higher energy states. Further, it was assumed that the carrier relaxation rate from the higher energy side to the lower energy side is proportional to the density of states on the low-energy side. We discuss the PL dynamics using the above rate equation (Equation (3)). The authors in ref. 41 assumed the carrier tunneling from relatively small QDs to relatively large QDs within a size distribution, and they did not consider the miniband formation and the presence of the localized states. Further, they focused only on the PL properties and assumed that $D(E)$ is a distribution obtained from the Gaussian fitting of their PL spectra. In the present CdTe QDSLs, the formation of minibands was verified experimentally from the results of the absorption spectra and detection energy dependence of the PLE spectra.^[33] Further, we modified the above model by assuming an exponential tail shape (Equation (2)) rather than a Gaussian function because we are considering the localized states on the low-energy side of the minibands. Finally, we calculated the PL dynamics using the Monte Carlo simulation based on the rate equation (Equation (3)).

Figure 5a shows the calculated PL dynamics with $\tau_r = 5.8$ ns, $\tau_t = 0.056$ ns, $E_{\max} = 2.177$ eV, and $\sigma = 27$ meV. The calculated PL decay depends significantly on the PL energy; the higher the PL energy is, the faster is the PL decay, which qualitatively explains the experimental results shown in Figure 2a. The time integration of the calculated result in Figure 5a yields the PL spectrum shown by the open circles in Figure 5b. The calculated PL spectrum shows the good agreement with the experimentally observed PL spectrum at 80 K (solid curve). The calculated PL energy dependencies of the decay profiles are shown in Figure 5c. The inset shows the calculated PL spectrum, and the down arrows represent the PL energies. Figure 5d shows the experimental (closed circles) and calculated (open triangles) results of the detection energy dependence of the PL decay time. The experimentally observed PL decay profiles in Figure 2a show a non-exponential decay. As mentioned above, the non-exponential decay of CdTe QDSLs can be analyzed by the sum of the stretched exponential and the single exponential functions; the calculated PL decay times are shown by the closed circles in Figure 5d. The calculated decay time (open triangles) was estimated from the slope of the calculated decay profiles as described in supporting information (Figure S3). The good agreement between the experimental and calculated results supports the validity of the PL mechanism of QDSLs proposed in this study.

Figure 6a shows the PL spectra and the second derivative of the absorption spectra of the 3D QDSLs at 80 K and 300 K. The miniband is formed near the absorption peak of the QDSLs, which corresponds to the minima of the second derivative spectra. The two dashed lines in Figure 6a indicate the lower and upper ends of the miniband formed in the 3D CdTe QDSLs, *i.e.*, the miniband width. The spectral width of the absorption spectra reflects the inhomogeneous width due to the size distribution of the QDs, which is sufficiently broader than the homogeneous linewidth of the individual QD levels. However, it should be noted that the low-energy shift of the absorption energy due to quantum resonance is observed in the present CdTe QDSLs. Since the inhomogeneous width of the absorption spectrum is larger than the change in the homogeneous linewidth of the QD levels with increasing temperature, the magnitude of the quantum resonance energy, *i.e.*, the miniband width, is not expected to increase much even if the homogeneous linewidth of the QD levels increases with increasing temperature. In fact, as shown in Figure S1, it is confirmed that (1) minibands are formed even at low temperatures and (2) there is no change in the detection energy dependence between low and room temperatures, *i.e.*, there is no clear temperature dependence. The difference between the absorption peaks of the CdTe QD solution sample and CdTe QDSLs is 37 meV, and it corresponds to the coupling energy attributed to the quantum resonance. Therefore, the miniband width is estimated to be 74 meV, which is twice the binding energy because the miniband width is determined by the energy difference between the bonding and anti-bonding states. The PL component in the energy region overlapping the above miniband width corresponds to the PL contributed from the miniband. Figure 6b shows the temperature-dependent intensity fraction of the PL component from the minibands (I_{miniband}) compared to the total PL (I_{total}). The PL component from the minibands increases with an increase in the temperature, reflecting the increase in the thermal activation from the localized state to the miniband. The open circles in Figure 6c denote the temperature-dependent PL decay time of the PL component from the minibands. The PL decay time increased with increasing the temperature.

In an ideal free exciton PL in a bulk crystal, an exciton with the exciton wave vector $\mathbf{K} = 0$ causes the emission, and the PL shows a delta-functional spectrum. However, an actual free exciton PL has a finite spectral width Δ due to phonon scattering, and the excitons distributed in the momentum space characterized by Δ contribute to the PL. Therefore, the effective exciton oscillator strength decreases and the exciton PL decay time increases with higher temperature. The exciton PL decay time is expressed as^[42-45]

$$\tau(T) \simeq \tau_0 \frac{1}{\zeta(T)}, \quad (4)$$

with

$$\zeta(T) = \frac{\int_0^{\Delta} D_{\text{ex}}(E) e^{-\frac{E}{k_{\text{B}}T}} dE}{\int_0^{\infty} D_{\text{ex}}(E) e^{-\frac{E}{k_{\text{B}}T}} dE}, \quad (5)$$

where τ_0 , $\zeta(T)$, $D_{\text{ex}}(E)$, and k_{B} denotes the exciton PL decay time at $T = 0$ K, the ratio of the number of excitons contributing to the PL over the total number of excitons, exciton density of states, and the Boltzmann constant, respectively. The temperature dependence of the PL decay time changes with the dimension of the system (d) because $D_{\text{ex}}(E)$ depends on d and is proportional to $E^{d/2-1}$. For 1D and 2D systems, the temperature dependence of the PL decay time can be obtained analytically: $\tau(T)$ is proportional to $T^{0.5}$ and $T^{1.0}$ for 1D and 2D systems, respectively.^[43] In one-dimensional systems such as quantum wires and one-dimensional arrangements of InAs QDs, the PL decay time increases in proportion to $T^{0.5}$;^[42-44] in GaAs quantum wells, which corresponds to a 2D system, the PL decay time increases in proportion to T .^[43] In a 3D system, Equation (5) cannot be solved analytically; the temperature dependence of the PL decay time must be obtained from numerical calculations. Zhong *et al.* reported that the temperature dependence of the PL decay time in a GaN bulk crystal is consistent with the results of numerical calculations based on Equations (4) and (5).^[45]

The solid curve in Figure 6c shows a numerically calculated curve for a 3D system with $\tau_0 = 0.017$ ns and $\Delta = 8$ meV, where fitting was performed using the least-squares method. In the temperature range of 80–220 K, the calculated results are in a good agreement with the experimental results (open circles). Above 240 K, the decay time becomes shorter than the calculated results. Figure 6d shows the temperature dependence of the integrated PL intensity normalized by the intensity at 80 K. In the temperature region below 220 K, the PL intensity is larger than ~80% of that at 80 K. Therefore, the experimentally observed decay time seems to reflect the radiative recombination lifetime. The PL intensity decreases with increasing the temperature due to a nonradiative recombination process. Therefore, the discrepancy between the experimental and calculated PL decay times in the high-temperature region can be attributed to the effect of the nonradiative recombination process.

The agreement between the experimental and calculated results below 220 K, where the effect of the nonradiative recombination process is small, indicates that the radiative recombination from a 3D extended exciton state exists in the QDSLs. This result strongly supports the formation of a 3D exciton state in the CdTe QDSLs. The formation of minibands by the quantum resonance was clearly confirmed from the viewpoint of the PL dynamics. In the inset of Figure 6c, the temperature dependence of the PL decay time is shown as a double-logarithmic plot, and it indicates that the PL decay time of the CdTe QDSL is proportional to

$T^{1.5}$. The dependence of $T^{1.5}$ is different from the results for 1D^[42-44] and 2D^[43] systems, demonstrating the formation of 3D excitonic states (minibands).

The in-plane QD density in the CdTe QDSLs can be controlled by changing the concentration of the QD solution used in the LBL assembly.^[33] Thus far, we demonstrated that 2D quantum resonances in the in-plane direction occur in the QD monolayers with the high in-plane QD density. Further, it is possible to fabricate the 1D QDSL by stacking QDs under the condition that the in-plane QD density is low. In the 1D QDSL, the quantum resonance occurs not in the in-plane direction but only in the stacking direction, that is, the 1D minibands are formed. Figures 7a and 7B show the second derivative of the absorption spectra and PL spectra of the CdTe QDSLs at 80 K and 300 K, wherein the 1D and 2D quantum resonances appear, respectively. The temperature dependence of $I_{\text{miniband}}/I_{\text{total}}$ in the 1D and 2D QDSLs is also shown in Figures 7c and 7d. The results show that the magnitude of $I_{\text{miniband}}/I_{\text{total}}$ becomes larger with increasing the temperature, which is similar to the case of the 3D QDSL. Figures 8a and 8b show the temperature-dependent PL decay time of the PL component from the minibands in the 1D and 2D structures. The solid curves show numerically calculated results using Equations (4) and (5) with $\tau_0 = 0.038$ ns and $\Delta = 4$ meV for 1D and $\tau_0 = 0.043$ ns and $\Delta = 9$ meV for 2D, respectively. The calculated results are in the good agreement with the experimental results (open rectangles and triangles). The inset shows the temperature dependence of the PL decay time in a double-logarithmic plot. The PL decay times of the 1D and 2D structures are proportional to $T^{0.5}$ and $T^{1.0}$, respectively, which again demonstrates the formation of 1D and 2D minibands.

3. Conclusion

The temperature dependence of the absorption and PL spectra and PL decay profiles were investigated systematically in the CdTe QDSLs with the 1D, 2D and 3D quantum resonance fabricated by the LBL method. The PL decay profiles became shorter with increasing the detection energy. Further, we calculated the PL dynamics based on the model that takes into account the miniband and weakly localized states (Anderson localized state) and quantitatively explained the results of the dependence of the PL decay profile on the detection energy.

We qualitatively explained that the magnitude of the Stokes shift decreases with increasing the temperature by considering the enhanced thermal activation process from the localized state to the miniband with increasing temperature. Furthermore, we observed a characteristic experimental result wherein the decay time from the miniband PL becomes longer in

proportion to $T^{1.5}$. This experimental result strongly supports the formation of 3D minibands in CdTe QDSLs. The $T^{0.5}$ and $T^{1.0}$ dependence of the PL decay times were confirmed for the QDSLs in which 1D and 2D quantum resonances occurred. The formation of minibands by the quantum resonance was clearly confirmed from the viewpoint of the PL dynamics. The results of this study will help clarifying further photoexcited dynamics in QDSLs with the minibands. Future studies on photophysical properties of QDSLs can be developed from the viewpoint of both fundamental and applied research by clarifying intra-miniband relaxation dynamics in QDSLs through transient absorption measurements and by studying the multiple exciton generation^[4,46] in QDSLs for the application to QD solar cells.

4. Experimental Section

We synthesized NAC-capped CdTe QDs by hydrothermal synthesis according to the previously reported procedure.^[30] First, 250 mg of tellurium powder (purity 99.99%; purchased from Kishida Chemical) and 312.5 mg of sodium borohydride (purity 98%; purchased from Kanto Chemical) were added to the vial. Then, 6 mL of deionized (DI) water was added to the vial and sealed, and the solution was cooled in an ice bath and reacted for ~ 8 hours. After the reaction, NaHTe, which is a tellurium ion source, is produced, and Na₂B₄O₇ precipitate. Next, 24 mM of NAC and 20 mM of Cd(ClO₄)₄·6H₂O (purity 99%; purchased from Fujifilm Wako Pure Chemical) were dissolved in 100 mL of DI water. Then, the pH of the solution was adjusted to 7.0 using 0.2 mM NaOH (purchased from Kishida chemical). Finally, 6.0 mM of the prepared NaHTe solution was added, and the pH was adjusted to 5.0 with a diluted HCl solution to prepare a CdTe QD precursor. After that, the NAC-capped CdTe QDs were synthesized by heating the precursor solution in an autoclave at 200 ° C for 8, 20, and 40 minutes. The mean radius (r) of the CdTe QDs synthesized with the reaction time of 8, 20, and 40 minutes are 1.4, 1.7, and 2.0 nm respectively. The QD solution with $r = 1.7$ nm was used to prepare QDSLs, and the QD solutions with $r = 1.4$ and 2.0 nm were used as the D-QDs and A-QDs to investigate the temperature dependence of the ET transfer rate. CdTe QDSLs were fabricated via LBL assembly.^[32,33,47-49] First, the quartz substrates were immersed in a piranha solution (98% H₂SO₄:30% H₂O₂ = 7:3, v/v) heated to 150 ° C for hydrophilic treatment to make the substrate surface negatively charged. Next, the substrates were alternately immersed in a diluted polydiallyl dimethylammonium chloride (PDDA) solution (20 wt% in H₂O; purchased from Sigma-Aldrich), which is a cationic polymer, and a diluted polyacrylic acid (PAA) solution ((~25%); purchased from FUJIFILM Wako Pure Chemical), which is an anionic polymer. In this process, the substrates were washed with DI

water before being immersed in a different solution. After preparing PDDA / (PAA / PDDA)₂ layers on the substrate, the substrates were immersed in a NAC-capped CdTe QDs solution. Because the NAC is negatively charged in water, the QD monolayer can be formed on the substrates. Additionally, QD multilayers were fabricated by alternately immersing the substrate in the PDDA solution and the CdTe QD solution. The CdTe QD multilayers (30 layers) were fabricated using a QD solution with $OD_{sol} = 0.20$ to produce the QDSLs in which 3D quantum resonance occurs in both the stacking and in-plane directions. Here, OD_{sol} is the optical density of the first absorption peak in the CdTe QDs solution in a cell with an optical path length of 10 mm. The average center-to-center distances between the QDs in the stacking and the in-plane direction, are 3.5 nm and 3.9 nm, respectively.^[33] Also, it was shown that if the in-plane QD distance is increased, that is, if the in-plane QD density becomes low, the quantum resonance in the in-plane direction is suppressed; the average surface-to-surface distance between QDs in the in-plane direction is 2.2 nm and 0.5 nm in the QD monolayer which is fabricated using a QD solution with $OD_{sol} = 0.02$ and 0.20, respectively.^[33] The CdTe QD multilayers (30 layers) in which 1D quantum resonance occurs only in the stacking direction were fabricated using a QD solution with $OD_{sol} = 0.02$. Furthermore, the QD monolayer in which 2D quantum resonance in the in-plane direction occurs was fabricated by using the QD solution of $OD_{sol} = 0.20$. In order to investigate the temperature dependence of the ET rate, we fabricated the bilayer structures using CdTe QDs with $r = 1.4$ and 2.0 nm. The bilayer structures were composed of three blocks; the monolayer of A-QDs with $r = 2.0$ nm, followed by the PDDA layer, and the monolayer of D-QDs with $r = 1.4$ nm. To measure the temperature dependence of the optical properties, the samples were attached to liquid-nitrogen variable temperature cryostats (Pascal POLL-500-P). Absorption spectra were recorded using a JASCO V-650 spectrometer with a spectral resolution of 0.2 nm. In PLE measurements, the excitation light was produced by a combination of a 100-W tungsten lamp and a monochromator. The emitted PL was analyzed by a photon counting method with a single monochromator. The spectral resolution was 0.5 nm. For the measurement of the PL spectra, a laser diode (405 nm, PicoQuant LDH-P-C-405) with a pulse width of 50 ps and a repetition of 80 MHz was used as an excitation source, and the PL was recorded using a Hamamatsu C10083CA fiber-coupled mini-spectrometer. The pump fluence was 50 pJ/cm². The laser diode with a pulse width of 50 ps and a repetition of 125 kHz was used as an excitation source for measuring the PL decay profiles. The PL decay profiles over long periods of several hundred nanoseconds were recorded by the time-correlated single photon counting method. The PL decay profiles with short time duration of less than 10 nanoseconds

were obtained using a Hamamatsu Photonics C5094 imaging spectrometer and a C4334 streak scope.

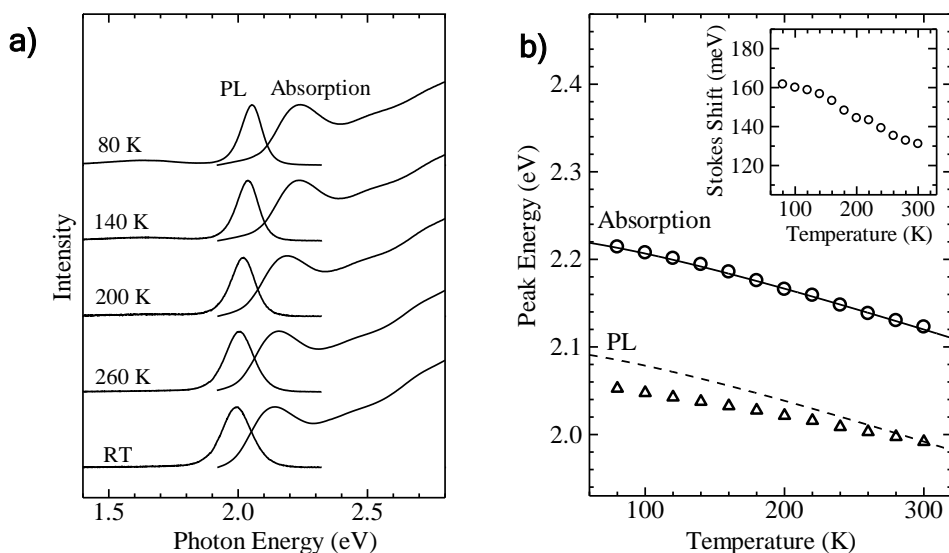


Figure 1. Temperature dependence of absorption and PL spectra of CdTe 3D QDSLs. (a) Absorption and PL spectra of CdTe QDSLs at 80 K, 140 K, 200 K, 260 K, and RT. (b) Temperature dependence of absorption peak energy (open circles) and PL peak energy (open triangles). The solid curve represents the result of the calculation by substituting $\alpha = 5.5 \times 10^{-4}$ eV/K and $\beta = 158$ K into Eq. (1). The dashed curve shows the calculation result for the temperature dependence of the PL peak energy with the same α and β the same values as in the analysis of the temperature dependence of the absorption peak energy were used. The inset shows the temperature dependence of the Stokes shift, which is the energy difference between the absorption and PL peak energies.

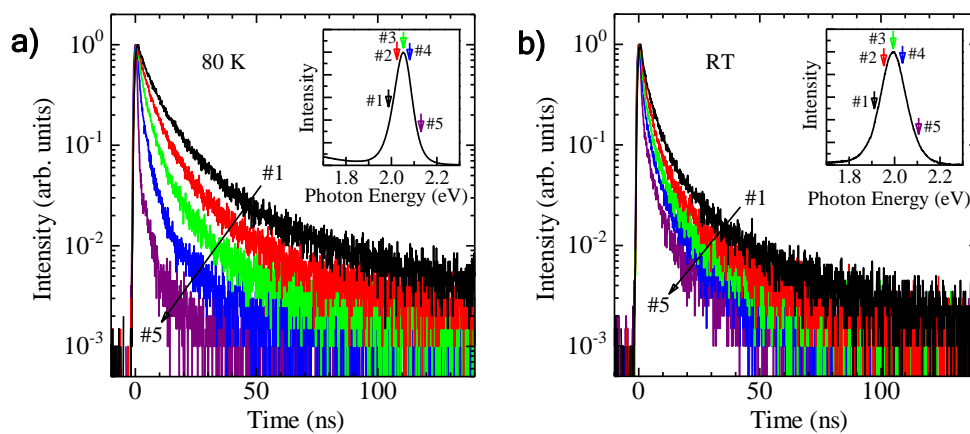


Figure 2. Detection energy dependence of PL decay profiles of 3D QDSLs at 80 K and RT. (a, b) Detection energy dependence of PL decay profiles at 80 K and RT. The insets show the PL spectra at 80 K and RT. The down arrows in the insets represent the detection energies and the arrow color corresponds to the color of the PL decay profiles.

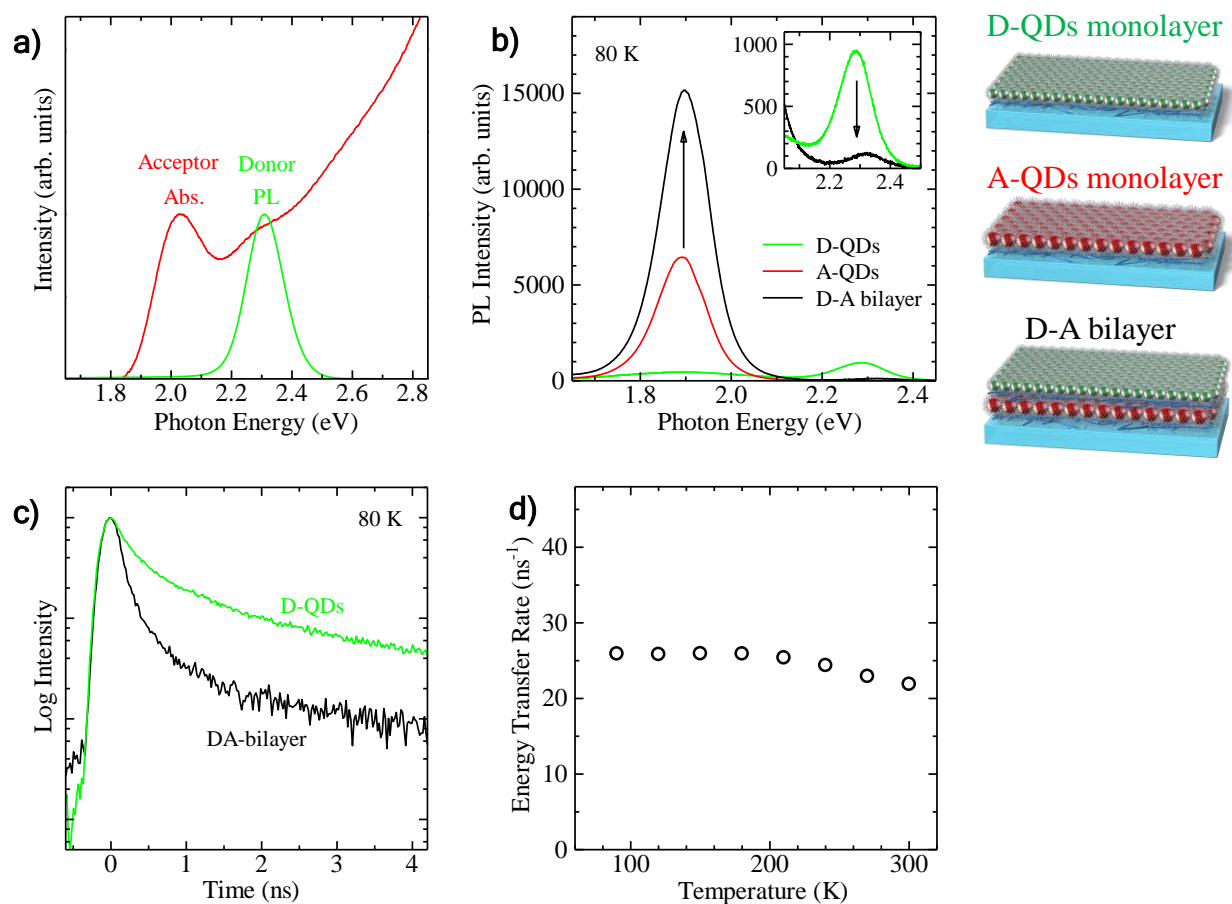


Figure 3. PL properties of the bilayer in which energy transfer occurs. (a) Absorption spectrum of the solution sample of CdTe QDs with a radius of 2.0 nm that act as energy acceptors (A-QDs) and PL spectrum of the solution sample of CdTe QDs with a radius of 1.4 nm that act as energy donors (D-QDs). (b) PL spectra of the monolayers of D-QDs and A-QDs, and the bilayer composed of D-QDs and A-QDs. The inset shows an enlarged view of the PL spectrum in the energy region corresponding to the PL of the D-QDs. (c) PL decay profiles of the monolayer of D-QDs and the bilayer at 80 K, detected at the PL peak of D-QDs. (d) Temperature dependence of the energy transfer rate estimated from the analysis of the PL decay profiles.

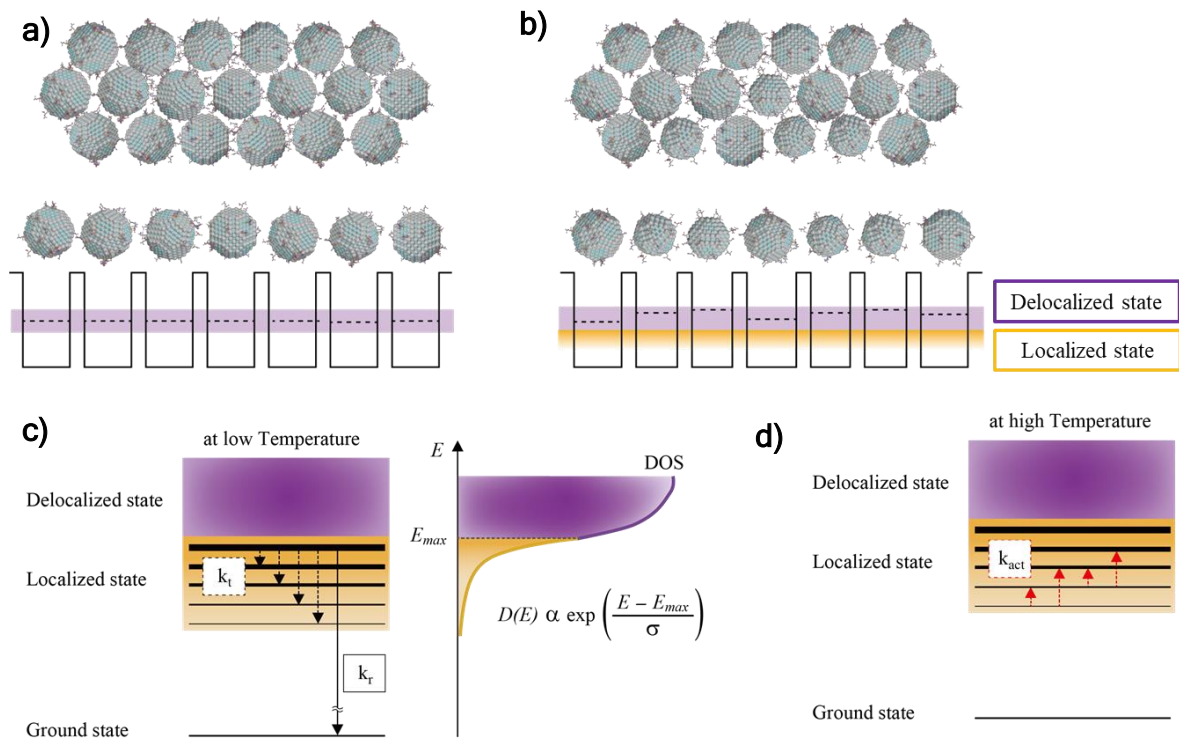


Figure 4. Schematics of the electronic states of the QDSLs with miniband formation and PL processes at low and high temperatures. (a) Schematics of the electronic states of ideal QDSLs where the QDs of uniform size are regularly arranged. The minibands are formed in the ideal QDSLs. (b) Schematics of the electronic states of real QDSLs in which there are irregularities because of the size distribution and disorder of the arrangement. In such cases, weak localization states—so-called Anderson localization states—are formed on the low-energy side of the minibands. The purple part shows delocalized states (minibands), and the yellow part shows weakly localized states. (c, d) PL process from the minibands and localized states at low and high temperatures. k_r , k_t , and k_{act} denote the recombination rate, tunneling rate, and thermal activation rate, respectively.

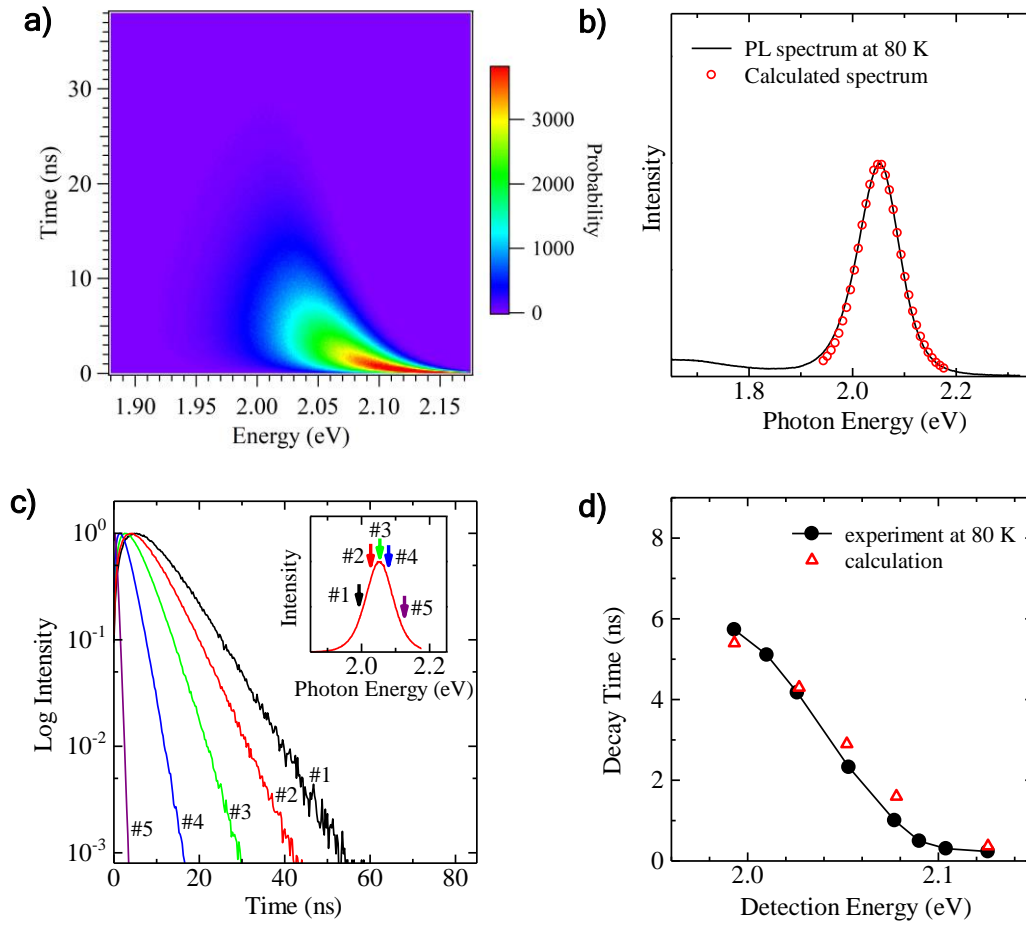


Figure 5. Calculated PL dynamics in 3D QDSLs. (a) PL dynamics calculated by the Monte Carlo simulation based on the rate equation (Eq. (3)) obtained by using the parameters of $\tau_r = 5.8$ ns, $\tau_t = 0.056$ ns, $E_{\max} = 2.177$ eV, and $\sigma = 27$ meV. (b) Open circles show the PL spectrum calculated by the time integration of the calculated result in Fig. 5a over the entire time region. The solid curve represents the experimental result of the PL spectrum at 80 K. (c) PL decay profiles obtained from the simulation results in Fig. 5a, where the inset shows the calculated spectrum and the down arrows represent the corresponding PL energy. (d) Experimental (closed circles) and calculated (open triangles) detection energy dependence of the PL decay time.

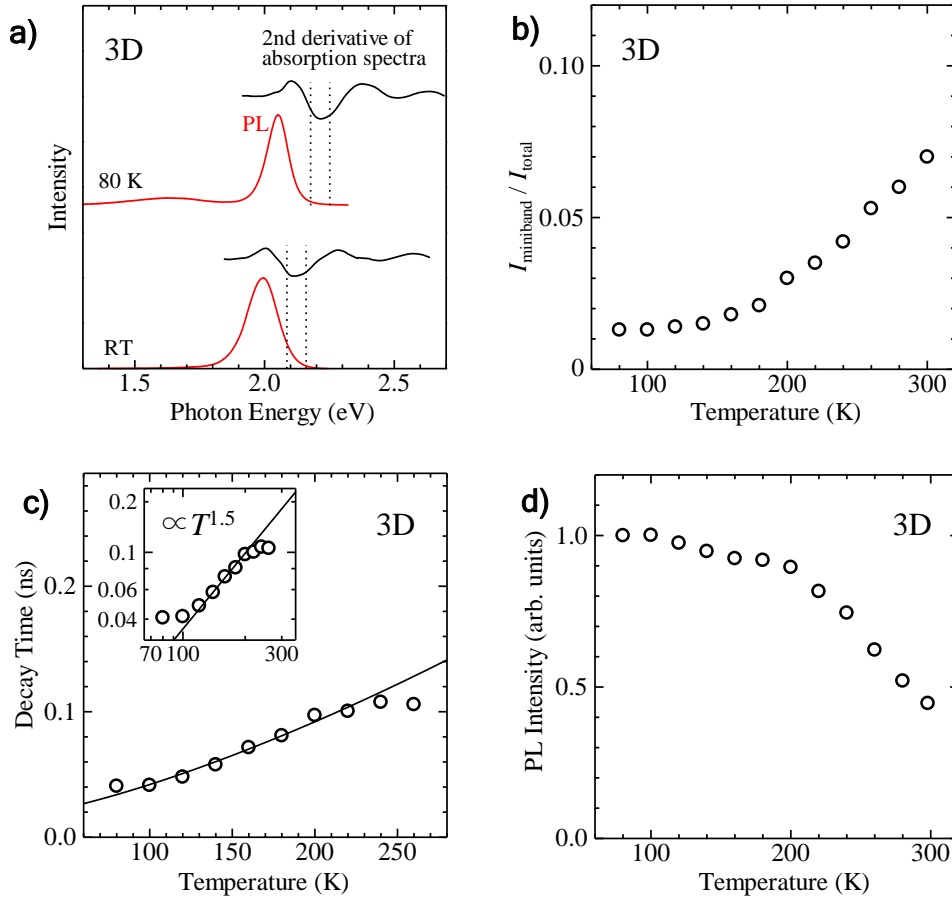


Figure 6. Temperature dependence of the PL properties of 3D CdTe QDSLs. (a) PL spectra and second derivative of the absorption spectra of QDSLs at 80 K and 300 K. The two dashed lines indicate the lower and upper ends of the miniband in CdTe QDSLs, *i.e.*, the miniband width. (b) Temperature-dependent intensity fraction of the PL component from the minibands (I_{miniband}) compared to the total PL component (I_{total}). (c) Temperature-dependent PL decay times of the PL component originated from the minibands. The solid curve shows a numerically calculated result for a 3D system using Eqs. (4) and (5) with $\tau_0 = 0.017$ ns and $\Delta = 8.0$ meV. In the inset, the temperature dependence of the PL decay time is shown as a double-logarithmic plot, which indicates that the PL decay time of QDSLs is proportional to $T^{1.5}$. (d) The temperature dependence of the integrated PL intensity normalized by the intensity at 80 K.

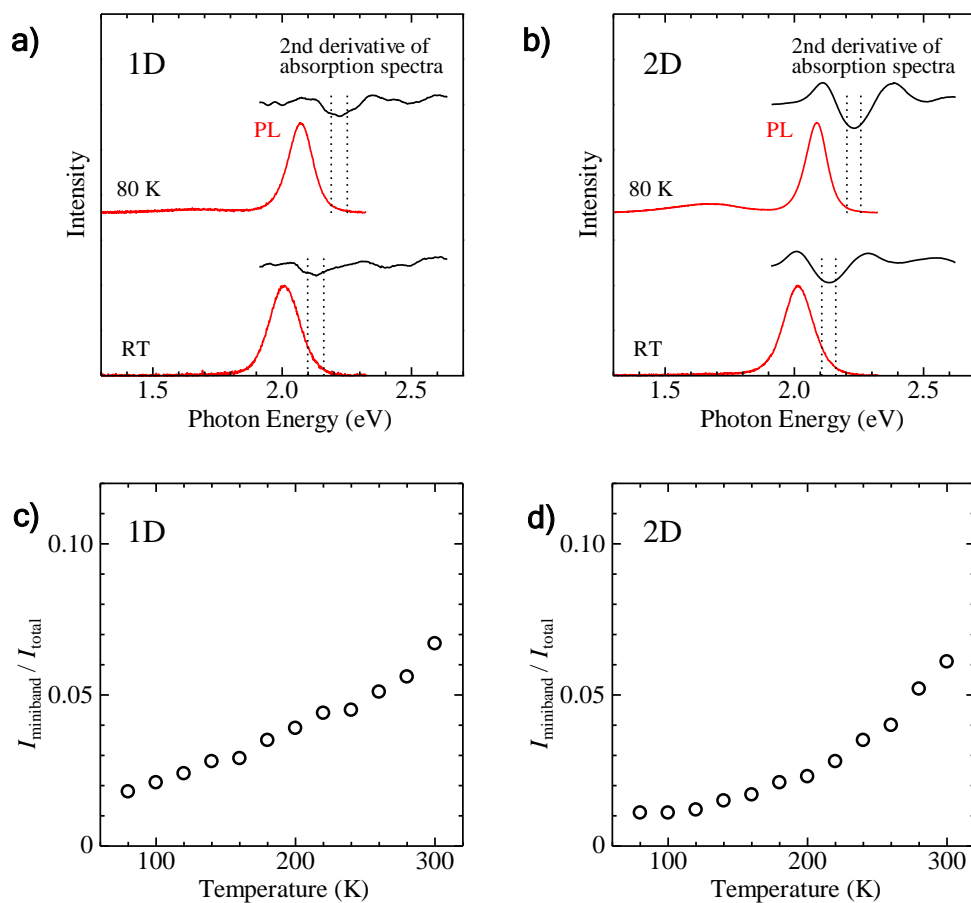


Figure 7. Temperature dependence of PL properties of 1D and 2D CdTe QDSLs. (a, b) PL spectra and second derivative of the absorption spectra of 1D and 2D QDSLs at 80 K and 300 K. The two dashed lines indicate the lower and upper ends of the miniband, *i.e.*, the miniband width. (c, d) Temperature-dependent intensity fractions of the PL component from the minibands (I_{miniband}) compared to the total PL component (I_{total}) for 1D and 2D QDSLs.

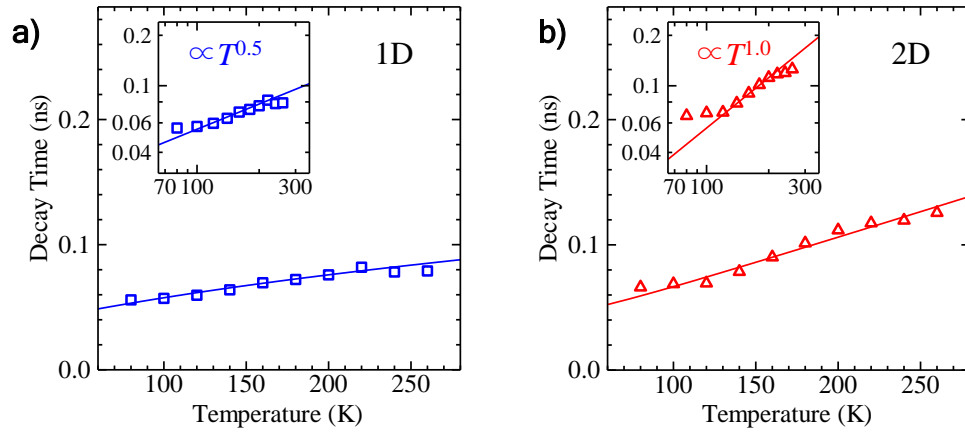


Figure 8. Temperature dependence of the PL decay times of 1D and 2D CdTe QDSLs. (a, b) Temperature-dependent PL decay times of the PL component originated from the minibands. The solid curve shows a numerically calculated result for the 1D and 2D systems using Eqs. (4) and (5) with $\tau_0 = 0.038$ ns and $\Delta = 4$ meV for the 1D system and with $\tau_0 = 0.043$ ns and $\Delta = 9$ meV for the 2D system. In the insets, the temperature-dependent PL decay times are shown as a double-logarithmic plot, which indicates that the PL decay times are proportional to $T^{0.5}$ (1D QDSL) and $T^{1.0}$ (2D QDSL).

Supporting Information

Detection energy dependence of PLE spectra at 80 K, 200 K, and RT, analysis of the PL decay profiles. Supporting Information is available from the Wiley Online Library or from the author.

Acknowledgements

K.H.-D. acknowledges Kusunoki 125, Grant-in-Aids for the Scientific Research from Japan Society for the Promotion of Science (KAKENHI), Grant No. 20K05419 and 18H05407, the Toyota Mobility Foundation, and the Masuya Research Foundation. D.K. acknowledges financial support from JSPS KAKENHI, Grant No. 20H02549.

Received: ((will be filled in by the editorial staff))

Revised: ((will be filled in by the editorial staff))

Published online: ((will be filled in by the editorial staff))

References

- [1] T. Hanrath, *J. Vac. Sci. Technol. A* **2013**, *30*, 030802.
- [2] I-Y. Chang, D. Kim, and K. Hyeon-Deuk, *ACS Appl. Mater. Interfaces* **2016**, *8*, 18321.
- [3] C. R. Kagan, C. B. Murray, *Nat. Nanotech.* **2015**, *10*, 1013.
- [4] I-Y. Chang, D. Kim, and K. Hyeon-Deuk, *ACS Appl. Mater. Interfaces* **2017**, *9*, 32080.
- [5] J.-S. Lee, M. V. Kovalenko, J. Huang, D. S. Chung, D. V. Talapin, *Nat. Nanotech.* **2011**, *6*, 348.
- [6] J.-H. Choi, A. T. Fafarman, S. J. Oh, D.-K. Ko, D. K. Kim, B. T. Diroll, S. Muramoto, J. G. Gillen, C. B. Murray, C. R. Kagan, *Nano Lett.* **2012**, *12*, 2631.
- [7] I. Gur, N. A. Fromer, M. L. Geier, A. P. Alivisatos, *Science* **2005**, *310*, 462.
- [8] O. E. Semonin, J. M. Luther, S. Choi, H.-Y. Chen, J. Gao, A. J. Nozik, M. C. Beard, *Science* **2011**, *334*, 1530.
- [9] G. H. Carey, A. L. Abdelhady, Z. Ning, S. M. Thon, O. M. Bakr, E. H. Sargent, *Chem. Rev.* **2015**, *115*, 12732.
- [10] H. Hosokawa, R. Tamaki, T. Sawada, A. Okonogi, H. Sato, Y. Ogomi, S. Hayase, Y. Okada, T. Yano, *Nat. Commun.* **2019**, *10*, 4.
- [11] G. Konstantatos, I. Howard, A. Fischer, S. Hoogland, J. Clifford, E. Klem, L. Levina, E. H. Sargent, *Nature* **2006**, *442*, 180.
- [12] R. Saran, R. J. Curry, *Nat. Photon.* **2016**, *10*, 81.
- [13] X. Tang, M. M. Ackerman, M. Chen, P. Guyot-Sionnest, *Nat. Photon.* **2019**, *13*, 277.
- [14] D. V. Talapin, C. B. Murray, *Science* **2005**, *310*, 86.
- [15] F. S. Stinner, Y. Lai, D. B. Straus, B. T. Diroll, D. K. Kim, C. B. Murray, C. R. Kagan, *Nano Lett.* **2015**, *15*, 7155.
- [16] E. Talgorn, Y. Gao, L. T. Kunneman, J. M. Schins, T. J. Savenije, M. A. van Huis, H. S. J. van der Zant, A. J. Houtepen, L. D. A. Siebbeles, *Nat. Nanotech.* **2011**, *6*, 733.
- [17] J. Jang, W. Liu, J. S. Son, D. V. Talapin, *Nano Lett.* **2014**, *14*, 653.
- [18] X. Lan, M. Chen, M. H. Hudson, V. Kamysbayev, Y. Wang, P. Guyot-Sionnest, D. V. Talapin, *Nat. Mater.* **2020**, *19*, 323.
- [19] C. B. Murray, C. R. Kagan, M. G. Bawendi, *Science* **1995**, *270*, 1335.
- [20] C. B. Murray, C. R. Kagan, M. G. Bawendi, *Annu. Rev. Mater. Sci.* **2000**, *30*, 545.
- [21] A. Dong, J. Chen, P. M. Vora, J. M. Kikkawa, C. B. Murray, *Nature*, **2010**, *466*, 474.
- [22] M. A. Boles, M. Engel, D. V. Talapin, *Chem. Rev.* **2016**, *116*, 11220.
- [23] S. J. Yoon, Z. Guo, P. C. dos Santos Claro, E. V. Shevchenko, L. Huang, *ACS Nano* **2016**, *10*, 7208.

- [24] J. Miyazaki, S. Kinoshita, *J. Phys. Soc. Jpn.* **2012**, *81*, 074708.
- [25] Y. Liu, M. Gibbs, J. Puthussery, S. Gaik, R. Ihly, H. W. Hillhouse, M. Law, *Nano Lett.* **2010**, *10*, 1960.
- [26] P. Reiss, J. Blueuse, A. Pron, *Nano Lett.* **2002**, *2*, 781.
- [27] H. Zhang, L. Wang, H. Xiong, L. Hu, B. Yang, W. Li, *Adv. Mater.* **2003**, *15*, 1712.
- [28] J. Guo, W. Yang, C. Wang, *J. Phys. Chem. B* **2005**, *109*, 17467.
- [29] A. L. Rogach, T. Franzl, T. A. Klar, J. Feldmann, N. Gaponik, V. Lesnyak, A. Shavel, A. Eychmüller, Y. P. Rakovich, J. F. Donegan, *J. Phys. Chem. C* **2007**, *111*, 14628.
- [30] H.-B. Bu, H. Kikunaga, K. Shimura, K. Takahashi, T. Taniguchi, D. Kim, *Phys. Chem. Chem. Phys.* **2013**, *15*, 2903.
- [31] L. Jing, S. V. Kershaw, Y. Li, X. Huang, Y. Li, A. L. Rogach, M. Gao, *Chem. Rev.* **2016**, *116*, 10623.
- [32] D. Kim, S. Tomita, K. Ohshiro, T. Watanabe, T. Sakai, I.-Y. Chang, K. Hyeon-Deuk, *Nano Lett.* **2015**, *15*, 4343.
- [33] T. Lee, K. Enomoto, K. Ohshiro, D. Inoue, T. Kikitsu, K. Hyeon-Deuk, Y.-J. Pu, D. Kim, *Nat. Commun.* **2020**, *11*, 5471.
- [34] Y. P. Varshni, *Physica* **1967**, *34*, 149.
- [35] J. Jouglar, C. Hetroit, P. L. Vuillermoz, and R. Triboulet, *J. Appl. Phys.* **1980**, *51*, 3171.
- [36] T. Watanabe, K. Takahashi, K. Shimura, D. Kim, *Phys. Rev. B* **2017**, *96*, 035305.
- [37] S. A. Crooker, J. A. Hollingsworth, S. Tretiak, V. I. Klimov, *Phys. Rev. Lett.* **2002**, *89*, 186802.
- [38] C. F. Klingshirn, *Semiconductor Optics, 4th ed.* (Springer, Berlin, 2012).
- [39] J. Werner, M. Peisl, *Phys. Rev. B* **1985**, *31*, 6881.
- [40] J. Yang and F. W. Wise, *J. Phys. Chem. C* **2015**, *119*, 3338.
- [41] A. Tackeuchi, Y. Nakata, S. Muto, Y. Sugiyama, T. Utsuki, Y. Nishikawa, N. Yokoyama, O. Wada, *Jpn. J. Appl. Phys.* **1995**, *34*, L1439.
- [42] D. S. Citrin, *Phys. Rev. Lett.* **1992**, *69*, 3393.
- [43] H. Akiyama, S. Koshihara, T. Someya, K. Wada, H. Noge, Y. Nahunura, T. Inoshita, A. Shimizu, H. Sakaki, *Phys. Rev. Lett.* **1994**, *50*, 8930.
- [44] A. Takahashi, T. Ueda, Y. Bessho, Y. Harada, T. Kita, *Phys. Rev. B* **2013**, *87*, 235323.
- [45] Y. Zhong, K. S. Wong, W. Zhang, D. C. Look, *Appl. Phys. Lett.* **2006**, *89*, 022108.
- [46] I.-Y. Chang, D. Kim, and K. Hyeon-Deuk, *J. Phys. Chem. C* **2019**, *123*, 2549.
- [47] G. Decher, *Science* **1997**, *277*, 1232.
- [48] A. Shavel, N. Gaponik, A. Eychmüller, *Eur. J. Inorg. Chem.* **2005**, *2005*, 3613.

[49] D. Kim, S. Okahara, M. Nakayama, Y. Shim, *Phys. Rev. B* **2008**, 78, 153301.